

Filamin A (16-23) reveals a hierarchy of unfolding forces arising from domain-domain interactions in the polyprotein chain

Tianyou Xu^{*}, Herbert Lannon^{*}, Sébastien Wolf^{*}, Fumihiko Nakamura⁺, and J. Brujić^{1*}

^{*}Department of Physics and Center for Soft Matter Research, New York University, 4 Washington Place, New York, NY, 10003, USA

⁺Translational Medicine Division, Department of Medicine, Brigham and Women's Hospital, Harvard Medical School, 75 Francis Street, Boston, MA, 02215, USA

¹Corresponding author. 608 Meyer Hall, 4 Washington Place, New York, NY, 10003, USA, Tel: (212)998-3586, Email: jb2929@nyu.edu

Abstract

The quaternary structure of Filamin A (FLNa) 16-23 was recently shown to exhibit multiple domain-domain interactions that lead to a propeller-like construction. Here we present single molecule force spectroscopy experiments to show a wide variety of mechanical responses of this molecule and compare it with its linear counterpart FLNa 1-8. The compact structure of FLNa 16-23 leads to a broad distribution of rupture forces and end-to-end lengths in the force-extension mode and multiple unraveling timescales in the force-clamp mode. Moreover, a subset of force-extension trajectories reveals a mechanical hierarchy in which the rupture of domain-domain interactions at high forces (>300 pN) liberates the unfolding of individual domains at low forces (~ 100 pN). This mechanism may also explain the order of magnitude difference in the rates of the biexponential fits to the distribution of unfolding dwell times under force-clamp. Overall, FLNa 16-23 under a force of 100 pN is more compliant than the linear FLNa 1-8. Since a physiological role of FLNa is to crosslink actin filaments, this range of responses allows it to accommodate a broad spectrum of forces exerted by the cell and its environment.

Key words: quaternary; filamin; single; molecule; force; spectroscopy

Introduction

Many proteins assemble into supramolecular structures in order to perform their biological function. For example, pilin monomers assemble into pili fibers that regulate bacterial locomotion (1–3), ankyrin repeats assemble into superhelical spirals that may influence neuronal function of the inner ear (4) and proteins aggregate into amyloid fibrils that impact the development of neurodegenerative diseases (5, 6). These complex structures have been characterized by single molecule force spectroscopy unveiling a diversity of mechanical behaviors. In the case of ankyrin repeats, α -helical domain-domain interactions lead to structures that are much more mechanically stable than the individual folds, inducing a hierarchy in their force response (4). Similarly, dimerization through β -sheet Ig domains Z1Z2 in titin leads to rupture forces as high as 700 pN that are significantly stronger than their unfolding force of ~ 170 pN (7). By contrast, stretching linear polyprotein chains, such as the tandem repeats in titin and ubiquitin, results in the unfolding of the individual domains in the order imposed by their mechanical stability (8, 9). Note that this order may be disrupted by the presence of stable intermediates within individual domains, as in the case of fibronectin (10). More generally, the specific force response of a given system reveals whether structural hierarchies are present and the nature of the underlying interactions.

A polyprotein molecule that has been shown to exhibit distinct mechanical architectures is FLNa (11). It is an actin-binding protein whose function is to crosslink the intracellular network of F-actin and regulate the remodeling of the cytoskeletal infrastructure (12–15). To achieve this function, it has been proposed that FLNa plays a role in mechanotransduction: it serves as an integrator capable of detecting mechanical changes and triggering appropriate biochemical reactions (16–19). The textbook view of the complex between two actin filaments and the dimer of FLNa is shown in Fig. 1, where domains 1-15 linearly bind to one actin filament and the clustered domains 16-24 bridge the gap between two adjacent actin filaments. These Ig domains interact in a pairwise manner and assemble into propeller-like structures (15, 20, 21). The inset shown in Fig. 1 illustrates the crystalline loop structure of FLNa 19-21, which specifically involves hydrogen bonding between the beta pleated A-strand in FLNa 20 and C-D strands in FLNa 21 (16). The unbinding of domains 20 and 21, which also occurs between domains 16-17 and 18-19, is predicted by molecular dynamics simulations to require ~ 50 pN of force (22), while the measured unfolding forces of linear 1-15 domains are in the range $\sim 100 - 200$ pN (23). Interestingly, recent

force-ramp experiments using magnetic tweezers reveal that FLNa 16-23 unravels at significantly lower pulling forces than the linear FLNa 1-15 (11). The molecular mechanisms by which the unraveling occurs and the effect of domain-domain interactions on the mechanical response of the protein remain open questions.

Using the atomic force microscope (AFM) here we investigate the force response of FLNa 1-8 and 16-23 over a broad range of forces in the force-extension mode, as well as the kinetics of unraveling under a constant stretching force. We collect a large statistical pool of data to show that both linear chain behavior and higher-order complexities coexist in the polyprotein. Features in the experimental distributions of rupture forces, end-to-end lengths and dwell times are then used to elucidate the mechanical hierarchies and their possible biological significance.

Materials and Methods

Fusion proteins were expressed in Sf9 cells (5108 cells) using Bac-to-Bac system (Invitrogen) in accordance with manufactures' instructions and the expressing cells were harvested 72 h post-infection. After washing with PBS, the cells were lysed in 40 mL of 20 mM sodium phosphate, pH 8.0, 1% Triton X-100, 300 mM NaCl, 20 mM imidazole, 1 mM mercaptoethanol, 2 mM PMSF, 10 g/ml aprotinin, and 10 g/ml leupeptin at 4°C. The extracts were centrifuged at 20,000g for 30 min at 4°C and loaded onto a Ni-NTA column (3 ml, Qiagen). The column was washed with washing solution (20 mM sodium phosphate, pH 8.0, 20 mM imidazole, 1 mM mercaptoethanol, 300 mM NaCl, 0.1% Triton X-100) and bound recombinant proteins were eluted with 20 mM sodium phosphate, pH 8.0, 300 mM imidazole, 1 mM mercaptoethanol. Purified proteins were concentrated using an Amicon Ultra-15 (Millipore) with a molecular weight retention of >5,000 Da and gel-filtered on Superdex 200 (10/300, GE Healthcare) column equilibrated with 50 mM Bicine-NaOH, pH 8.3 and 0.1 mM mercaptoethanol. Recombinant proteins were stored at -80°C.

AFM measurements were conducted using a custom-built apparatus consisting of a modified Digital Instruments detector head (AFM-689, Veeco Instruments, Santa Barbara, CA) and a three dimensional piezoelectric translator, with a range of 5 μ m and a resonant frequency of \sim 10 kHz (P-363.3CD, Physik Instrumente, Karlsruhe, Germany). Laser position and alignment were performed using a photo-diode at 100 kHz (Schafter Krichhoff). Details of the AFM and its operation modes have been described else-

where (24, 25). Silicon nitride cantilevers (MLCT, Bruker Probes, Camarillo, CA) were used, with spring constants calibrated using the equipartition theorem. An aliquot of 10-15 μL of poly-protein (0.10 mg/mL, Bicine-NaOH buffer pH 8.3) was deposited on an evaporated gold surface and immobilized for 10 minutes. The solution was then washed with PBS buffer of pH 8.3. All experiments were performed at room temperature. Poly-protein chains were picked from the surface by non-specific binding the the AFM tip. Chains were then pulled at a constant velocity or constant force, depending on the mode of operation. The experiment is regulated by a PID controller and run using software written in Igor PRO. Any trace that has at least three unfolding events, defined by sharp staircases or sawteeth in the two modes, is then analyzed. This gives reasonable experimental certainty that the Ig chain has been picked.

The quantitative analysis of the traces involves fitting the worm-like chain (WLC) model defined by,

$$F(x) = \frac{k_B T}{L_p} \left(\frac{1}{4} \left(1 - \frac{x}{L_c} \right)^{-2} - \frac{1}{4} + \frac{x}{L_c} \right) \quad (1)$$

where x is the extension in the end-to-end length of the molecule, L_p is the persistence length and L_c is the contour length (26, 27). For the fitting, L_p is fixed to be the size of one amino acid of ~ 0.37 nm. In the case of force-extension data, we measure the peak-to-peak distance ΔL_{FX} associated with each rupture event in the sawtooth pattern. The unfolding of a domain gives rise to ΔL_{FX} that corresponds to the contour length of the molecule L_c minus its folded length L_f . Since L_c is given by the number of amino acids times the size of an amino acid and L_f of Ig domains is estimated to be ~ 3.7 nm (28), we can deduce whether rupture events correspond to the unfolding of individual domains. In the case of force-clamp data, the step size ΔL_{FC} is compared to the value of x in the WLC model at the particular force of 100 pN minus the folded length L_f .

Results and Discussion

In Fig. 2, A and B we show trajectories of FLNa 1-8 under a constant velocity of 400 nm/s and a constant force of 100 pN. Domains 1-8 behave as linear polyprotein chains, as seen in previous AFM studies of FLNa 1-15 (23). Each peak of the sawtooth represents the unfolding of a domain in the chain, while the last peak is the detachment of the chain from either the cantilever tip or the gold surface. The WLC fits to the sawteeth reveal peak-to-peak distances in the range $\Delta L_{FX} = 27 - 33$ nm, similar to the predicted

values shown in Table 1 (29). Moreover, the steps in the unfolding staircase in the range $\Delta L_{FC} = 25 - 27$ nm correspond to the predicted extensions of Ig domains listed in the table. The average unfolding force of ~ 200 pN coincides with that of the 27th Ig domain in titin (30), which predicts an unfolding timescale of ~ 0.05 s⁻¹ using the Bell model (31). Indeed, the force-clamp trajectory in Fig. 2 B unravels on the predicted timescale.

By contrast, in Fig. 3 we show a gallery of responses to force in FLNa 16-23. Typical trajectories in FLNa 16-23 can be classified into two categories: those that exhibit a broad distribution of end-to-end lengths at similar rupture forces, shown in Fig. 3, A and B, and those that display a reverse mechanical hierarchy in which the strong interactions break before weak ones, shown in Fig. 3, C and D. More specifically, Fig. 3 A shows rupture events at ~ 150 pN where seven out of the nine peaks have ΔL_{FX} outside of the range of the unfolding of individual domains. This result is in agreement with the broad range of step sizes in the analogous constant force trajectory at 100 pN in Fig. 3 B. Moreover, the observed rupture force of ~ 150 pN corresponds to an unraveling of the molecule on a timescale of 1s⁻¹ under force-clamp, which is an order of magnitude faster than the unfolding staircase in Fig. 2 B. In the cases shown in Fig. 3, A and B the FLNa 16-23 is significantly weaker than its linear counterpart FLNa 1-8. Since the contour length of the whole FLNa 16-23 is ~ 240 nm, which is only slightly longer than the observed trajectory in Fig. 3 A, these events must involve the unfolding of the individual Ig domains. A possible explanation for the weaker unfolding as well as the breadth of the released lengths is that the direction along which the force is applied to each domain is imposed by the packing of the Ig domains within the polyprotein chain, as shown in the propeller-like structure proposed in (20). Indeed, changing the linkage between a tandem of linear ubiquitin monomers was found to change the rupture forces and released lengths according to the pulling direction (32).

The second category of typical FLNa 16-23 responses under the same experimental conditions reveals strong rupture events followed by weak ones in the force-extension mode and multiple unraveling timescales in the force-clamp mode, as shown in Fig. 3, C and D. In particular, Fig. 3 C shows three rupture forces at ~ 200 pN that are approximately twice as strong as those that follow. The inset shows that the frequency of trajectories with n liberated low force peaks decreases with n . Similarly, Fig. 3 D shows the constant force unraveling of three strong events over 3 s, followed by the rapid succession of three weak events in only 0.7 s. These observations suggest that the weak events are initially hidden from the applied force within the protein superstructures and only subsequently released.

Next, we analyze the statistics of all the collected trajectories. The histograms of rupture forces and peak-to-peak distances in ΔL_{FX} for FLNa 16-23 at constant velocity reveal notable differences compared to the results found in previous studies on FLNa 1-15 (23). The force distribution ($N = 850$ events) in Fig. 4 A spans a much broader range than that of FLNa 1-15 (shaded histogram) and reaches values higher than the unfolding force of any known mechanically stable protein (33). These rupture forces on the order of 700 pN are comparable to the unbinding of the quaternary structure of Ig domains Z1Z2 in titin (7). In addition, the low force regime probed by magnetic tweezers broadens the rupture force distribution all the way down to 5 pN (11). The inset shows that a power law tail captures the experimental distribution. This scale-free force response to the extension of the end-to-end length makes this protein uniquely adaptable to a wide range of external perturbations. Likewise, the distribution of ΔL_{FX} in Fig. 4 B is much broader than the shaded histogram found in Ig 1-15, indicative of the proteins' complex response to force. Note that the lengths span from extensions of short intermediate or domain-domain ruptures of ~ 5 nm up to the extension of multiple domains of ~ 90 nm.

Despite the broad distributions observed in FLNa 16-23, the probability map of ΔL_{FX} as a function of the rupture force in the inset reveals a peak in the region that corresponds to the linear unfolding lengths of Ig domains (~ 28 nm) at rupture forces between 100 – 150pN, in agreement with the unfolding forces of weaker domains in FLNa 1-15. A filtered histogram of ΔL_{FX} in Fig. 4 C for only those events that occur after a rupture force that is at least twice as high as their rupture force isolates the same unfolding peak at 28nm. The fact that the probability map for this reduced data set is consistent with domain unfolding, as shown in the inset, means that the rupture of higher order structures linearizes the polyprotein chain and liberates Ig domain unfolding.

Force-clamp data at 100 pN on the two protein constructs reveals a distribution of step sizes for FLNa 16-23 ($N = 830$ events) in Fig. 4 D and a single peak at ~ 22 nm for FLNa 1-8 ($N = 372$ events) in the inset. These results are consistent with force extension distributions for the two constructs. The broad distribution of step sizes in FLNa 16-23 exhibits a peak at ~ 20 nm, which is roughly consistent with the unfolding lengths of the individual domains. While the force-extension mode probes structures with broad interaction energies, pulling at a constant force isolates only those that are susceptible to the applied force in the time window of the experiment, i.e. 5 seconds. For this reason, it is harder to distinguish unfolding events from domain-domain ruptures according to the order in which they

occur. Instead, we consider the timescales on which the unraveling of the end-to-end length occurs.

To study the kinetics of the unraveling processes of FLNa 1-8 and 16-23 we analyze the distribution of dwell times for each step in the staircases observed under force-clamp. In the case of linear FLNa 1-8, the fact that the step sizes are uniform implies that averaging and normalizing the staircases in the extended length is equivalent to plotting a cumulative distribution of dwell times (CDF) to the unfolding events, as shown in Fig. 5. Although the variability in the step lengths in the case of FLNa 16-23 may violate this equivalence, data analysis shows that they are the same. This result means that averaging over all the staircases gives a distribution of step lengths that is homogeneous over time.

Fitting the distribution then gives the functional form for the kinetics of unfolding (34). The CDF of dwell times $F(t)$ and the normalized end-to-end length are constructed from staircases lasting at least 2.75 seconds to optimize the size of the data set and the accuracy of the fit. For both constructs the empirical distributions are fit with biexponential functions,

$$F(t) = 1 - Ae^{-a_1 t} - (1 - A)e^{-a_2 t} \quad (2)$$

where a_1 and a_2 are the rate constants and A is the weight of the populations associated with each rate. We find that both rate constants are faster in the FLNa 16-23 construct, while A remains the same between the polyproteins, as indicated in the figure legend. It is interesting to note that the two rate constants show a clear separation in timescales since a_1 is ten times slower than a_2 for both constructs. While the two rates may be associated with the weak and strong domains unfolding in linear FLNa 1-8 (also seen in the bimodal force distribution in Fig. 4 A), the molecular origin of the two populations is more complex in FLNa 16-23, as suggested by the broad step size distribution. For example, it is possible that the population that is slow to unravel represents interdomain interactions, while the faster population corresponds to domain unfolding. This simplified view of the process agrees with the observation that unfolding forces identified in FLNa 16-23 are weaker than those in FLNa 1-8. Overall, these mechanisms lead to a more compliant response to force by FLNa 16-23, which releases $\sim 70\%$ of its length after 2.75 seconds, while the more resilient FLNa 1-8 only releases $\sim 50\%$.

Conclusion

Our results from force-extension and force-clamp data are indicative of domain-domain interactions between Ig domains in FLNa 16-23 that are not present in the linear FLNa 1-8. These domain-domain interactions lead to compact geometries that alter the pulling direction of each domain and thus lead to a broad distribution of extended lengths and rupture forces. Moreover, globular structures involving multiple domain-domain interactions are stronger than the force of individual domain unfolding. These interactions sequester individual domains from the applied force, such that linear domain unfolding occurs after their rupture. As a result, they induce multiple timescales in the unfolding trajectories under a constant stretching force.

In Fig. 6, we show the linear and the quaternary structure of FLNa 16-23, inspired by the recent findings in (20, 21). The maximum extension one could achieve by extending the folded chain is ~ 30 nm in Fig. 6 A. On the other hand, the shortest extension from rupturing domain-domain interactions is on the order of the length of a single domain of ~ 4 nm, depending on the geometry of the arrangement with respect to the pulling direction, as shown by the arrows in Fig. 6 B. Strong domain-domain interactions allow the protein to withstand higher pulling forces and shield the individual domains from the applied force. The released lengths then vary according to the topology of the compact globule. The multiplicity in the possible interactions offers an explanation for the broad range of forces we observe, while the number of distinct configurations accounts for the diversity in the end-to-end lengths.

Despite the complexity of possible polyprotein arrangements, we find a strong correlation between the force response of those events that are released after the rupture of a high force and those of individual Ig domains. We thus conclude that strong domain-domain interactions, such as those identified in Ig domains in titin (7), need to be broken in order to unfold the linear polyprotein chain. It is interesting to note that ankyrin domains form supramolecular structures that behave like Hookean springs and rupture at similarly high forces (4).

Biologically, this broad range of interactions in the Filamin A dimer allows it to accommodate both weak and strong mechanical stresses in the environment. Experimentally it is clear that the non-actin binding domains have a higher complexity than those that bind to actin, which leads to their larger compliance in response to a stretching force and a scale-free distribution of rupture forces. It is plausible that domains 16-23 are the first to rearrange, or even unfold, in order to keep the stiffer cross-linked

actin intact. Indeed, it has been shown that the partial rearrangement of the compact globule of FLNa 16-23 triggers biochemical pathways that may serve as part of the mechanical feedback system of the cell (19). The advantage of studying entire segments of Filamin A is that they portray the macroscopic response inside the cellular machinery. However, this is at the expense of knowing the specifics of the underlying molecular interactions. In future work, the complexity in Filamin A may be dissected by cloning specific pairs of domains to enumerate the mechanisms through which the protein responds to force.

Acknowledgements

We would like to thank Michael Sheetz for seeding this project at the National University of Singapore and Lea-Laetitia Pontani for a careful reading of the manuscript. J. B. holds a Career Award at the Scientific Interface from the Burroughs Wellcome Fund and was supported in part by New York University Materials Research Science and Engineering Center Award DMR-0820341 and a Career Award 0955621.

References

1. Andersson, M., E. Fallman, B. E. Uhlin, and O. Axner, 2006. Dynamic Force Spectroscopy of *E. coli* P Pili. *Biophysical Journal*. 91:2717-2725.
2. Biais, N., D. L. Higashi, J. Brujić, M. So, and M. P. Sheetz, 2010. Force-dependent polymorphism in type IV pili reveals hidden epitopes. *Proc. Natl. Acad. Sci. USA*. 107:11358–11363.
3. Alegre-Cebollada, J., C. L. Badilla, and J. M. Fernandez, 2010. Isopeptide Bonds Block the Mechanical Extension of Pili in Pathogenic *Streptococcus pyogenes*. *Journal of Biological Chemistry*. 285:11235–11242.
4. Lee, G., K. Abdi, Y. Jiang, P. Michaely, V. Bennett, and P. E. Marszalek, 2006. Nanospring behaviour of ankyrin repeats. *Nature*. 440:246–250.
5. Ganchev, D. N., N. J. Cobb, K. Surewicz, and W. K. Surewicz, 2008. Nanomechanical Properties of Human Prion Protein Amyloid as Probed by Force Spectroscopy. *Biophysical Journal*. 95:2909–2915.

6. Kellermayer, M. S. Z., L. Grama, Á. Karsai, A. Nagy, A. Kahn, Z. L. Datki, and B. Penke, 2005. Reversible Mechanical Unzipping of Amyloid-Fibrils. *The Journal of Biological Chemistry*. 280:8464–8470.
7. Garcia-Manyes, S., C. L. Badilla, J. Alegre-Cebollada, Y. Javadi, and J. M. Fernandez, 2012. Spontaneous Dimerization of Titin Protein Z1Z2 Domains Induces Strong Nanomechanical Anchoring. *Journal of Biological Chemistry*. 287:20240–20247.
8. Oberhauser, A. F., P. K. Hansma, M. Carrion-Vazquez, and J. M. Fernandez, 2001. Stepwise unfolding of titin under force-clamp atomic force microscopy. *Proc. Natl. Acad. Sci. USA*. 98:468–472.
9. Brujić, J., R. Hermans, K. A. Walther, and J. M. Fernandez, 2006. Single-molecule force spectroscopy reveals signatures of glassy dynamics in the energy landscape of ubiquitin. *Nature Physics*. 2:282–286.
10. Oberhauser, A. F., C. Badilla-Fernandez, M. Carrion-Vazquez, and J. M. Fernandez, 2002. The Mechanical Hierarchies of Fibronectin Observed with Single-molecule AFM. *Journal of Molecular Biology*. 319:433–447.
11. Chen, H., X. Zhu, P. Cong, M. P. Sheetz, F. Nakamura, and J. Yan, 2011. Differential mechanical stability of filamin A rod segments. *Biophysical Journal*. 101:1231–1237.
12. D’Addario, M., P. Arora, R. P. Ellen, and C. A. McCulloch, 2002. Interaction of p38 and Sp1 in a mechanical force-induced, 1 integrin-mediated transcriptional circuit that regulates the actin-binding protein filamin-A. *Journal of Biological Chemistry*. 277:47541–47550.
13. Tseng, Y., K. M. An, O. Esue, and D. Wirtz, 2004. networks. *Journal of Biological Chemistry*. 279:1819–1826.
14. Ehrlicher, A., F. Nakamura, J. H. Hartwig, D. Weitz, and T. P. Stossel, 2011. Mechanical strain in actin networks regulates FilGAP and integrin binding to filamin A. *Nature*. 478:260–263.
15. Nakamura, F., T. M. Osborn, C. A. Hartemink, J. H. Hartwig, and T. P. Stossel, 2007. Structural basis of filamin A functions. *Journal of Cell Biology*. 179:1011–1025.

16. Pentikäinen, U., and J. Yläanne, 2009. The Regulation Mechanism for the Auto-Inhibition of Binding of Human Filamin A to Integrin. *Journal of Molecular Biology.* 393:644–657.
17. Woo, M. S., Y. Ohta, I. Rabinovitz, T. P. Stossel, and J. Blenis, 2004. Ribosomal S6 kinase (RSK) regulates phosphorylation of filamin A on an important regulatory site. *Molecular Cell Biology.* 24:3025–3035.
18. Glogauer, M., P. Arora, D. Chou, P. A. Janmey, G. P. Downey, and C. A. McCulloch, 1998. The role of actin-binding protein 280 in integrin-dependent mechanoprotection. *Journal of Biological Chemistry.* 273:1689–1698.
19. Kainulainen, T., A. Pender, M. D’Addario, Y. Feng, P. Lekic, and C. A. McCulloch, 2002. Cell Death and Mechanoprotection by Filamin A in Connective Tissues after Challenge by Applied Tensile Forces. *Journal of Biological Chemistry.* 277:21998–22009.
20. Tossavainen, H., O. Koskela, P. Jiang, J. Yläanne, I. D. Campbell, I. Kilpeläinen, and P. Permi, 2012. Model of a Six Immunoglobulin-Like Domain Fragment of Filamin A (1621) Built Using Residual Dipolar Couplings. *Journal of the American Chemical Society.* 134:6660–6672.
21. Ruskamo, S., R. Gilbert, G. Hofmann, P. Jiang, I. D. Campbell, J. Yläanne, and U. M. Pentikäinen, 2012. The C-terminal rod 2 fragment of Filamin A forms a compact structure that can be extended. *Biochemical Journal (Immediate Publication).* xx:xx–xx.
22. Chen, H. S., K. S. Kolahi, and M. R. Mofrad, 2009. Phosphorylation Facilitates the Integrin Binding of Filamin under Force. *Biophysical Journal.* 97:3095–3104.
23. Furuike, S., T. Ito, and M. Yamazaki, 2001. Mechanical unfolding of single filamin A (ABP-280) molecules detected by atomic force microscopy. *FEBS Letters* 498:72–75.
24. Oberhauser, A. F., P. E. Marszalek, H. P. Erickson, and J. M. Fernandez, 1998. The molecular elasticity of the extracellular matrix protein tenascin. *Nature.* 393:181–185.
25. Fernandez, J. M., and H. Li, 2004. Force-Clamp Spectroscopy Monitors the Folding Trajectory of a Single Protein. *Science.* 303:1674–1678.

26. Bustamante, C., J. Marko, E. Siggia, and S. Smith, 1994. Entropic elasticity of lambda phage DNA. *Science*. 265:1599–1600.
27. Bouchiat, C., M. D. Wang, J. Allemand, T. Strick, S. M. Block, and V. Croquette, 1999. Estimating the Persistence Length of a Worm-Like Chain Molecule from Force-Extension Measurements. *Biophysical Journal*. 76:400–413.
28. Lad, Y., T. Kiema, P. Jiang, O. T. Pentikäinen, C. H. Coles, I. D. Campbell, D. A. Calderwood, and J. Yläanne, 2007. PDB 2J3S. Structure of three tandem filamin domains reveals auto-inhibition of ligand binding. *EMBO Journal*. 26:3993–4004.
29. Reorganizing the protein space at the Universal Protein Resource. 2012. *The UniProt Consortium*. 40:D71–D75.
30. Carrion-Vazquez, M., A. F. Oberhauser, S. B. Fowler, P. E. Marszalek, S. E. Broedel, J. Clarke, , and J. M. Fernandez, 1999. Mechanical and chemical unfolding of a single protein: A comparison. *Proc. Natl. Acad. Sci. USA*. 96:3694 – 3699.
31. Bell, G., 1978. Models for the specific adhesion of cells to cells. *Science*. 200:618–627.
32. Ke, C., Y. Jiang, M. Rivera, R. L. Clark, and P. E. Marszalek, 2007. Pulling Geometry-Induced Errors in Single Molecule Force Spectroscopy Measurements. *Biophysical Journal*. 92:L76–L78.
33. Valbuena, A., J. Oroza, R. Hervasa, A. M. Veraa, D. Rodrígueza, M. Menendezb, J. I. Sulkowskac, M. Cieplakc, and M. Carrion-Vazquez, 2009. On the remarkable mechanostability of scaffoldins and the mechanical clamp motif. *Proc. Natl. Acad. Sci. USA*. 106:13791–13796.
34. Brujić, J., R. I. Hermans, S. Garcia-Manyes, K. A. Walther, and J. M. Fernandez, 2007. Dwell-Time Distribution Analysis of Polyprotein Unfolding Using Force-Clamp Spectroscopy. *Biophysical Journal*. 92:2896–2903.

FLNa Segment	Range of the Number of Amino Acids	Range of the Estimated Peak-to-Peak Distance ΔL_{FX} (nm)	Range of the Estimated Step Size ΔL_{FC} at 100 pN
1-8	93 - 103	30.71 - 34.41	25.69 - 28.78
16-23	82 - 99	26.64 - 32.93	22.28 - 27.54

Table 1: Length characteristics of domains in FLNa 1-8 and 16-23. We list the number of amino acids (UniProt database), estimated range of peak-to-peak distances and polypeptide chain extension at 100 pN for both constructs.

Figure Legends

Figure 1

Dimerization of two FLNa monomers. The actin binding domain (ABD) anchors the protein to the actin. Linear repeats 1-15 (segment 1) exhibit strong interactions, while FLNa 16-23 (segment 2) displays less affinity with the actin filament. Dimerization occurs between Ig 24 of two adjacent FLNa proteins.

Figure 2

A typical force-extension trace at a constant velocity of 400 nm/s in (A) and a force-clamp trace at a constant force of 100 pN in (B) for the linear construct FLNa 1-8.

Figure 3

Distinct mechanical behaviors of FLNa 16-23. The diversity in the lengths unraveled at a constant velocity of 400 nm/s is shown in (A) and at a constant force of 100 pN in (B). Other traces reveal strong rupture events occurring before weak ones such as in example (C), which manifests itself as a separation of timescales in the constant force unraveling in (D).

Figure 4

Histograms of rupture forces in (A) and peak-to-peak distances in (B) for all the traces of FLNa 16-23 pulled at a constant velocity. Probability map in the inset reveals the breadth of interactions within the molecule. (C) The distribution of peak-to-peak distances for events that occur after a high rupture force is similar to the unfolding of linear domains, as confirmed by the force-extension probability map in the inset. (D) The step-size distribution under force-clamp of FLNa 16-23 is broader than that of FLNa 1-8 in the inset.

Figure 5

Empirical CDFs for the dwell times and the normalized end-to-end length of FLNa 1-8 and 16-23 at a pulling force of 100 pN. Data is fit with a biexponential function in Eq. (2) (FLNa 1-8: $a_1 = 0.1 \pm 0.03s^{-1}$ $a_2 = 1.9 \pm 0.5s^{-1}$ $A = 0.75 \pm 0.1$; FLNa 16-23: $a_1 = 0.3 \pm 0.08s^{-1}$ $a_2 = 3.1 \pm 0.7s^{-1}$ $A = 0.71 \pm 0.1$).

Figure 6

Examples of hypothetical arrangements of Ig domains 16-23. (A) Arrangement of the domains in a linear polyprotein chain. (B) The known interactions in FLNa 16-23 are incorporated into a globular configuration.

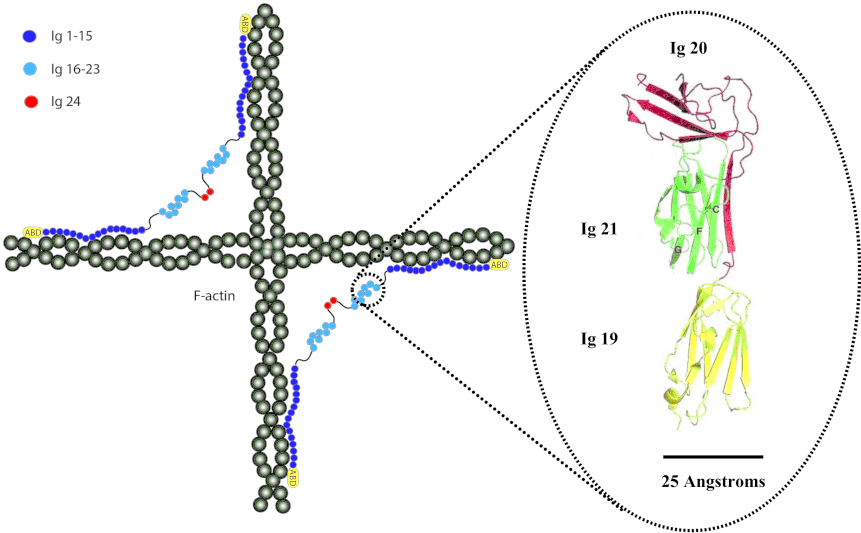


Figure 1:

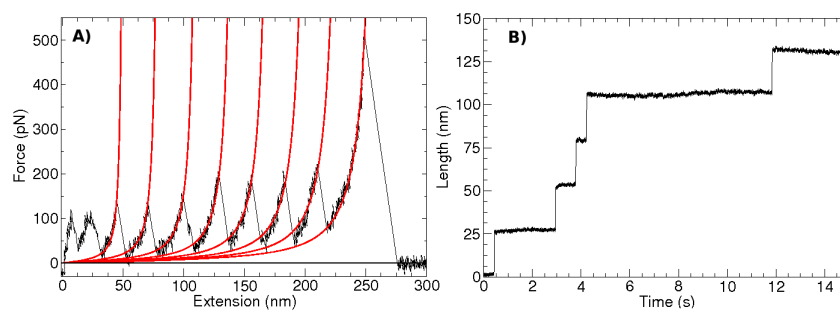


Figure 2:

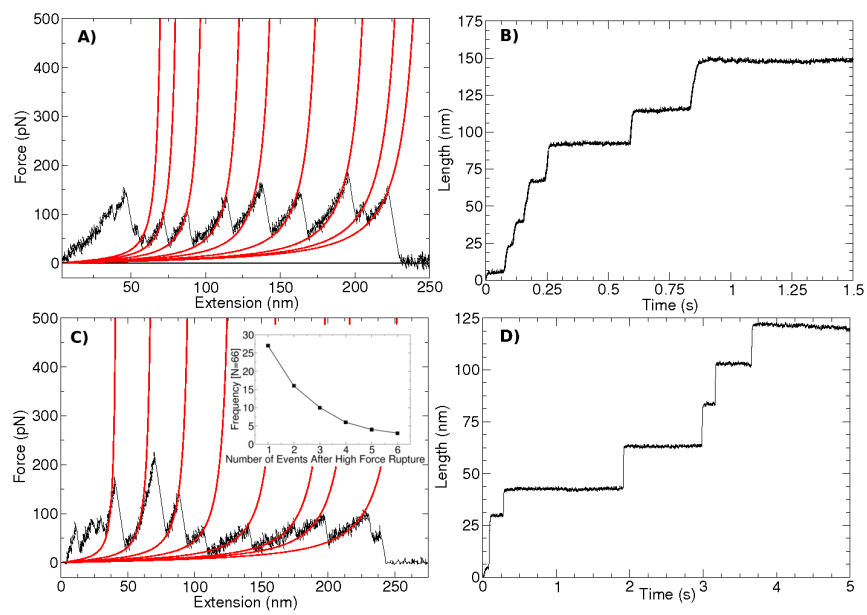


Figure 3:

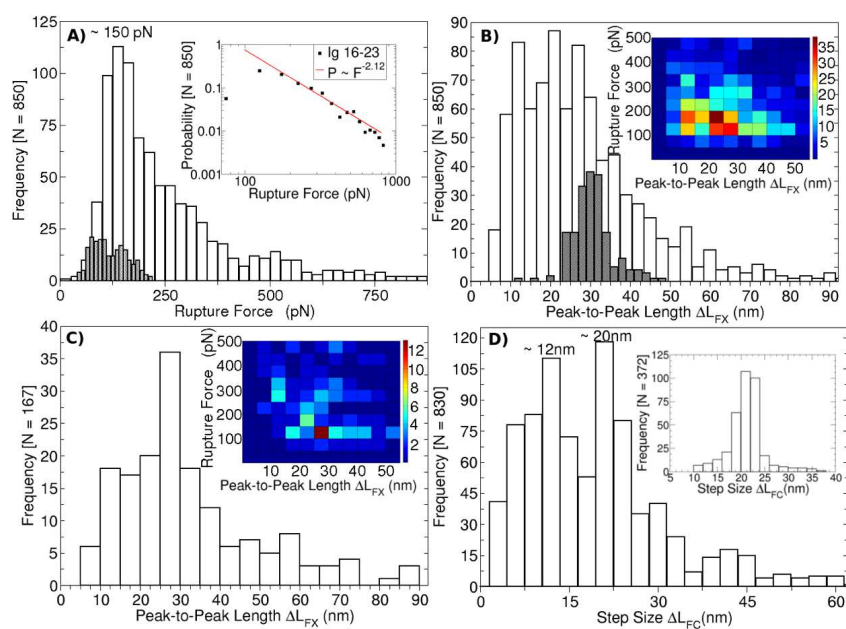


Figure 4:

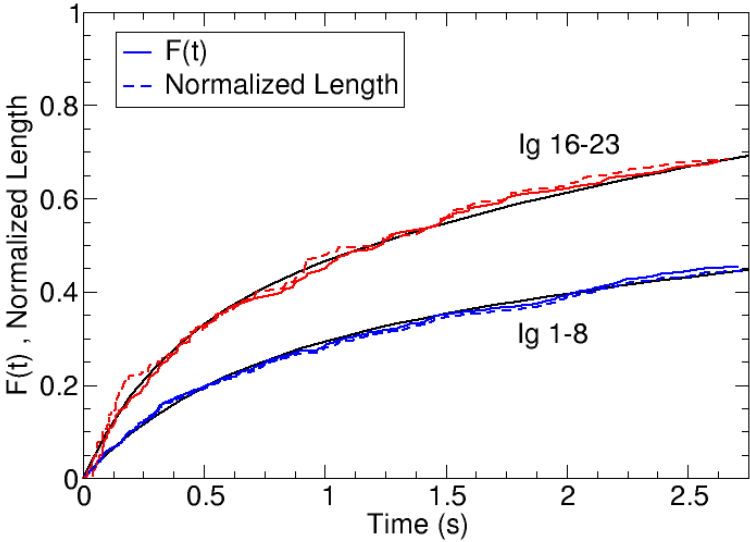


Figure 5:

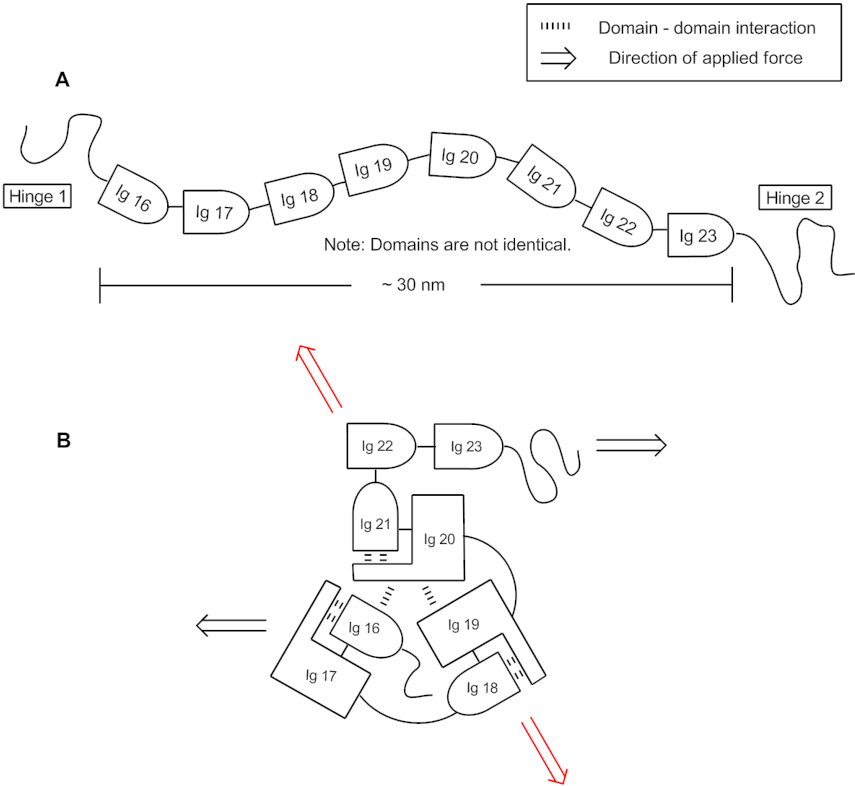


Figure 6: